RETURN VALUE ESTIMATES OF SIGNIFICANT WAVE HEIGHT BASED ON A NEW NORWEGIAN HINDCAST (NORA10)
-
(PRELIMINARY RESULTS)

Ole Johan Aarnes, Magnar Reistad, Øyvind Breivik and Hilde Haakenstad
Norwegian Meteorological Institute

1. INTRODUCTION

In offshore engineering return value estimates of significant wave height (H_s) often play a crucial role in dimensioning e.g. structures and anchorage. Industries like offshore renewable energy, shipping and the oil industry are dependant on a safe operation, preferably to a minimum cost. It is therefore important to establish accurate extreme estimates, applicable today and in the near future, in order to prevent casualties, environmental accidents or even loss of lives.

Several studies have been made on this topic, often based on some time series, either *in-situ* or hindcast data, for one or a limited number of locations. Today, data coverage is increasing both in time and space, allowing extreme analysis on H_s to be taken one step further.

Caires and Sterl (2005) based their analysis on the ERA40 global reanalysis developed by the European Centre for Medium-Range Weather Forecast (ECMWF), see Uppala *et al.* (2005). With 6-hourly data fields covering a total of 45 years and a 1.5° x 1.5° spatial resolution, this archive provides a valuable data set for global extreme estimates of H_s. But, as the ERA40 reanalysis is known to underestimate the peak values of H_s (Caires and Sterl, 2003), their extreme estimates was corrected using a simple linear relation between the estimated H_s100 (100-year return value) based on the ERA40 data and buoy observations, respectively. The paper concluded that the estimated H_s100 were less reliable in the storm track regions of the high latitudes, where the estimates seemed excessively high, peaking at around 24.5-27.5m south of Iceland. Results are accessible at www.knmi.nl/waveatlas/.

Besides numerical models, altimetry is really the only other source of data as of today that offers relatively high spatial information on significant wave height. The poor temporal resolution of the polar orbiting satellites is however a big drawback. Still, the data have proven valuable in extreme analysis. Alves and Young (2003) used a combination of Geosat, Topex/Poseidon and ERS-1 data spanning a period of 10 years (1986-1995) to obtain global estimates of the H_s100. Using two different methods in their calculations, i.e. the combination of statistical distribution and selection of a data sub-set, they found the highest estimates to reach about 25m South and Southwest of Iceland. However, it was concluded that the goodness-of-fit between the cumulative (CDF) and empirical (EDF) density function was poor in the same region, probably producing too high H_s100 estimates.

To recapitulate, the procedure commonly used for estimating H_s100 may be summarized by three different aspects of the analysis. First, one needs to determine a subset of the initial data to be included in the calculations. Two, an appropriate statistical mode, i.e. CDF, needs to be established. Three, the method of fitting the chosen CDF to the data, i.e. the estimators of the CDF, must be decided. In spite of numerous efforts, there does not seem to exist a universally accepted approach, superior of the rest. Mathiesen *et al.* (1994) proposed a recommended practice for extreme wave analysis, fitting a three-parameter Weibull distribution to peaks-over-threshold (POT) data, which is a frequently used combination. The POT method only retains peak values above some fixed threshold. Alternatively, one may use the complete sample of data, a.k.a Initial Distribution Method (IDM). Both approaches were used in Alves and Young (2003), but combined with two different CDF's, the three-parameter Weibull distribution and the Gumbel distribution. Caires and Sterl (2005) also used the POT method, but combined with the exponential distribution.

Intuitively, one would expect to find the most sever wave conditions in the Southern Ocean, where the global mean is at its highest. However, both papers presented above proved otherwise. Statistically the roughest sea states are found in the North Atlantic, making it a attractive area for extreme analysis on H_s100. The Norwegian Meteorological Institute has recently completed a regional hindcast-study that covers this part of the world's oceans. The NORA10 is based on the ERA40 reanalysis, but has an increased temporal and spatial resolution, see Reistad *et al.* (2007), which benefits the performance of the model. Here, the 45 year long archive will be exploited to find estimates of the H_s100.

In the following, we give a brief presentation of the data in chapter 2. Chapter 3 presents the method used in the extreme analysis. Chapter 4 gives a short validation of significant wave height obtained from the NORA10 and the ERA40 versus observations, while chapter 5 offers discussion and conclusions.

2. DATA

a. ERA40 data

The ERA40 is the latest fully completed reanalysis available from the European Centre for Medium Range Weather Forecasting (ECMWF). This comprehensive meteorological archive includes both atmospheric and wave data, covering a total of 45 years, i.e. Sep. 1957 – Aug. 2002, hereon referred to as the ERA40 period. The reanalysis was carried through with the ECMWF's Integrated Forecasting System (IFS), i.e. a coupled atmosphere-wave model, very similar to the one used operationally, but with lower resolution. The data fields are available every 6 hours with a 1.5° x 1.5° spatial resolution. The ERA40 is well documented in Uppala et al. (2005).

b. NORA10 data

NORA10 (NOrwegian ReAnalysis 10 km) is the newest hindcast developed by The Norwegian Meteorological Institute, see Reistad *et al.* (2007). This regional hindcast is based on the ERA40 reanalysis, but run with a higher temporal (3h) and spatial (10km) resolution. The two reanalysis cover the same period, in addition the NORA10 is continually being extended and currently also covers the period Sep. 2002 – 2008. Only data from the ERA40 period will be used in the following analysis.

Atmospheric forcing is obtained with the HIRLAM 10 km, see Bjørge (2003). Temperature, wind velocity, specific humidity and liquid water in the boundary zone are relaxed towards ERA40, while some of the large-scale features are maintained using a digital filter. Sea surface temperatures are interpolated from the ERA40 or the ice data archive at The Norwegian Meteorological Institute.

A modified version of the WAM cycle 4 has provided the wave data, see Komen *et al.* (1994). A 10 km version of the model is run on the same model domain and grid as the HIRLAM10, and nested inside a larger 50 km WAM-model, see Figure 1. All in all, the NORA10 covers the Northeast-Atlantic, including the North Sea, The Norwegian Sea and the Barents Sea.

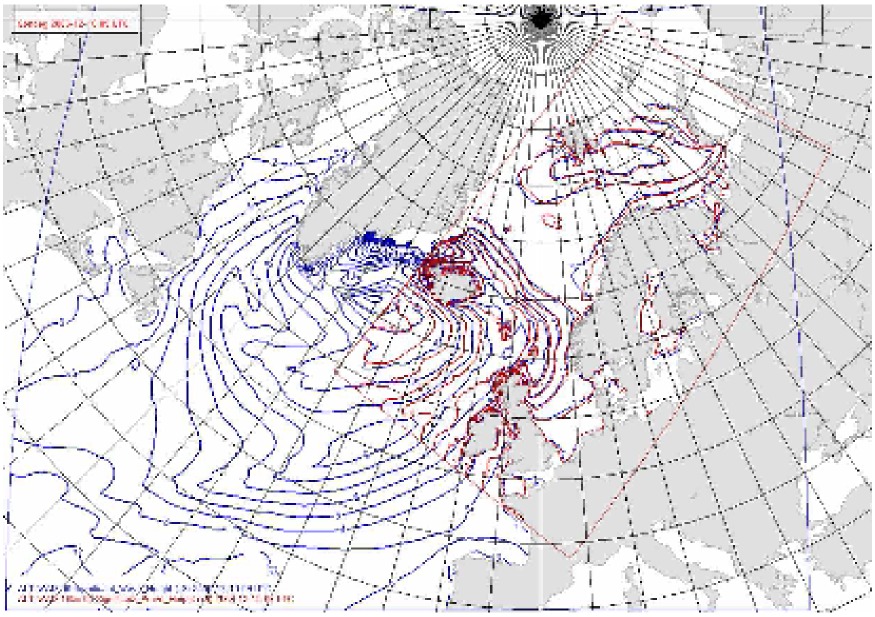

Figure 1: Model domains: The HIRLAM10 and WAM10 model domain are shown in red, i.e. the hindcast area. The WAM50 model domain is shown in blue.

c. Observations

In the following analysis we use a selection of *in-situ* measurements covering the Northeast Atlantic Ocean, see Figure 2. The data set is a collection of buoy and platform measurements covering all together the period August 1991 – August 2002. Each individual time series varies in length, ranging from half a year to slightly above 9 years. The data have been quality controlled using a routine that looks for outliers in monthly time series as explained in Saetra and Bidlot (2004). In addition, all obvious wrong data have been removed through visual inspection. All observations are 4h means (±2h) centred around synoptic times, i.e. 00, 06, 12 and 18UTC.

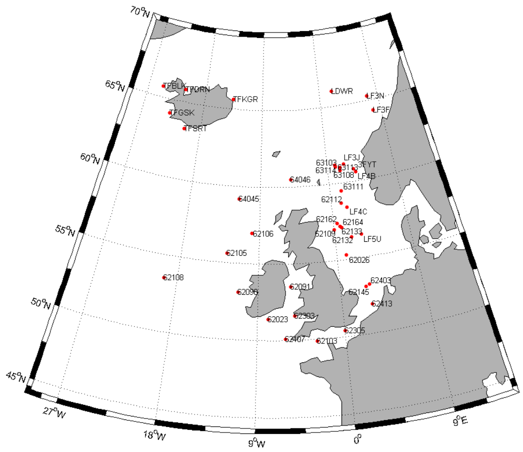

Figure 2: The available *in-situ* measurements used in the analysis is a collection of buoy and platform readings covering the Northeast Atlantic Ocean.

While most platforms are permanently fixed to one location, some buoys are subjected to movement. Here we have only used data within an area of +/- 0.2° of the median latitude and +/- 0.4° of the median longitude of the individual time series. So, data originating from areas with slightly different wave climatology are coarsely filtered out, meaning the time series contain gaps. This may also be a result of missing data or filtered spike values.

3. METHOD OF ANALYSIS

As stated in the introduction, an important element of extreme analysis is selecting the data most representative for the parameter you want to foresee, i.e. the H_s maxima.

The initial distribution method (IDM) utilizes all available data. Calm periods are included with the same weight as periods of rough seas. A single storm is often represented by more than one entry depending on the sampling frequency. With short time series, this might be the only option. However, the method itself contradicts an important assumption in extreme value theory, i.e. each entry is assumed independent. This is certainly not the case for 3- or 6-hourly data. Still, the method has been used extensively, often with acceptable results.

In order to get around the conditionality of independent data, a form of resampling of the data is necessary. This may be done in several of ways, one being the annual maximum method (AM), i.e. extracting only the highest value per year. This certainly guarantees an uncorrelated data set, but severely reduces the total number of data, often reducing the reliability of the extreme estimate. One should also keep in mind that some years may produce more than one severe storm, while other years are relative calm. Still, with this method, only one entry is sampled per year.

There are two well-known alternative methods going around the problem with AM. These are the *r*-largest order statistics and the peaks-over-threshold method (POT). The former only samples a fixed number (*r*) of the highest values per year, in that way increasing the total number of entries and not censoring those years with higher waves. A more common approach is the POT method, where only peaks above some fixed threshold is retained. However, one storm may occasionally produce two peaks with only a few hours apart. In order for the data to be uncorrelated it is necessary to impose an additional restriction, i.e. excluding any peaks closer than a given period of time of the local maximum. In the following analysis we will apply the POT method excluding peaks less than 48h apart. This is in line with Caires and Sterl (2005).

Depending on the methods discussed above, the chosen subsets of data belong to different families of distribution. IDM, AM and the r-largest statistics all retain data that theoretically should conform to one out of three distributions, Frechet, Gumbel and Weibull, i.e. the generalized extreme value family (GEV). POT-data on the other hand belong to the generalized Pareto distribution (GP), e.g. the exponential distribution, see Coles (2001). Still, earlier work show that POT-data is combined with CDF's which descend from the GEV-family, see e.g. Alves and Young (2004) and Mathiesen *et al.* (1994).

In the following analysis, we apply the Gumbel distribution (Fisher Tippert Type 1), fitted to data obtained with the POT and IDM method. The Gumbel distribution has an upper tail asymptotic to the exponential distribution, however, in practice it is difficult to tell where the upper tail commences (WMO, 1998), so we apply the Gumbel distribution. In comparisons, Caires and Sterl (2005) used a combination of POT and the exponential distribution.

The Gumbel distribution, F, is given by

$$F(x) = \exp\left\{-\exp\left[\frac{-(x-A)}{B}\right]\right\}, \tag{1}$$

where F is the CDF of the variable x, e.g. H_s. A and B are estimated using the method of moments (MOM), defined by

$$A = \bar{x} - \gamma B \tag{2}$$

$$B \approx \sqrt{6}\frac{s}{\pi}, \tag{3}$$

where $\bar{x}$ and s^2 are the mean and the variance of x, respectively, and γ=0.5771 is the Euler's constant. Taking the logarithm of eq. 1 and rearranging we are left with

$$h = A + B[-\ln(-\ln F)]\,. \tag{4}$$

The return value of interest, i.e. H_s100, is estimated using eq. (4) with the proper probability value $F=F_R$, which is dependant on the temporal resolution of the data. Using a data set with an average of N_y events per year will have the probability of not exceeding the R-year return value represented by

$$F_R = 1 - \frac{1}{R \times N_y}\,. \tag{6}$$

From eq. (4), h plotted against -ln(-ln F) offer a linear representation of the CDF intercepting A with the slope B. This probability plot is a good visual tool to determine how well the theoretical distribution conforms to the data. In the following, we assume each event of the data subset to represented the likelihood

$$f = \frac{1}{N+1} \tag{5}$$

, where N is the total number of entries.

With the POT method, N will vary with the chosen threshold, which also affects the H_s100. In the following we will use three different thresholds, i.e. the 85- , 90- and 95-percetile of the initial data set, heron referred to as POT85, POT90 and POT95. The most appropriate data subset obtained with IDM, POT85, POT90 and POT95 will be determined visually using the probability paper.

4. RESULTS

a. Model validation

In Reistad (2007), a model validation of the NORA10 was presented at two locations in the North Sea and the Norwegian Sea, i.e. Ekofisk for the period 1990-1992 and 2000-2001 and Draugen for the period 2000-2001. Here, we present supplementing results of significant wave height. Since the NORA10 is based on the ERA40, it is of interest to address the gain in value of running a regional hindcast versus a global hindcast, so we include an identical validation of the ERA40.

Figure 3 presents three regression plots of H_s obtained with the NORA10 and the ERA40 versus observations, respectively, and the two hindcasts together. Clearly the performance of the NORA10 is higher than that of the ERA40. Besides the higher correlation, 0.95 versus 0.93, the regression line of the NORA10 coincides almost perfectly with the 1:1 line. In contrast, the ERA40 clearly underestimates H_s. It should be mentioned that the ERA40 reanalysis is run with a deep-water model and does not account for bottom topography, unlike the NORA10. This will certainly influence the performance of the hindcast in coastal areas where bottom friction becomes effective. It may be debated whether some of the observations should have been excluded for validation purposes, e.g. the five locations found around Iceland and buoy 62303, see Figure 2. However, the results only underline the benefit of running a regional hindcast with high resolution and bottom topography, opposed to a global deep-water model. Table 1 provides all verification results of the NORA10 and ERA40 compared to the available observations.

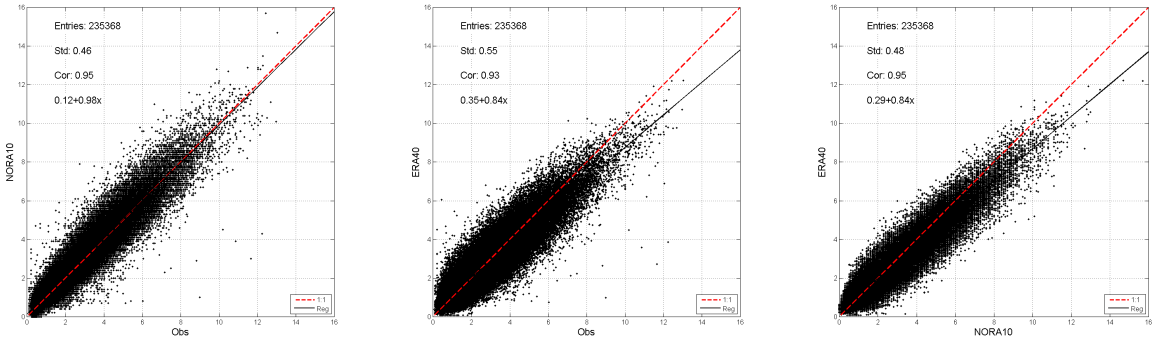

Figure 3: Scatter diagrams of significant wave height. Left: observation vs. NORA10. Middle: Observation vs. ERA40. Left: NORA10 vs. ERA40.

Table 1: Verification results of the NORA10 and ERA40 compared to *in-situ* measurements, buoys and platforms. Location is represented by the buoy/observation number. n_t is the total number of available data. r is the correlation coefficient. y gives the regression line. The N-th percentile is the 95- and 99-percentile of all available data.

Location	Position	n_t	r			$y = ax + b$						Nth-Percentile					
			Buoy NORA10	Buoy ERA40	NORA10 ERA40	Buoy NORA10		Buoy ERA40		NORA10 ERA40		Buoy		NORA10		ERA40	
						a	b	a	b	a	b	95th	99th	95th	99th	95th	99th
3FYT	60.80N 3.40E	8156	0,93	0,86	0,93	1,12	-0,04	0,83	0,46	0,75	0,46	4,9	6,2	5,7	7,4	4,9	6,2
62023	51.40N 7.90W	3672	0,97	0,94	0,93	0,98	-0,06	0,98	0,45	0,96	0,57	4,5	6	4,5	5,7	5,1	6,5
62026	55.40N 1.20E	5313	0,96	0,94	0,96	1,04	-0,16	0,87	0,05	0,81	0,21	3,7	4,9	3,9	5	3,4	4,4
62090	53.10N 11.20W	1937	0,97	0,97	0,98	1,16	-0,06	1,05	0,17	0,88	0,28	5,2	6,8	6,1	8	5,7	7,7
62091	53.50N 5.40W	1925	0,95	0,87	0,88	1,28	-0,33	0,94	0,1	0,71	0,37	2,5	3,2	3,1	4	2,8	3,8
62103	49.90N 2.90W	13526	0,93	0,91	0,92	1,06	0,16	1,06	0,39	0,93	0,34	3,5	4,6	4	5,4	4,3	5,7
62105	55.50N 13.00W	5903	0,97	0,97	0,98	0,97	-0,07	0,86	0,19	0,87	0,32	6,7	8,9	6,5	8,6	6,1	8,1
62106	57.00N 9.90W	9389	0,97	0,97	0,98	1,01	-0,12	0,87	0,17	0,85	0,33	6,5	8,4	6,5	8,7	5,9	7,9
62107	50.10N 6.10W	8779	0,95	0,95	0,97	0,93	0,2	0,99	0,29	1,02	0,16	4,9	6,3	4,9	6,2	5,3	6,8
62108	53.50N 19.50W	6410	0,97	0,97	0,98	0,87	0	0,86	0,15	0,96	0,22	6,9	9,4	6,2	8,4	6,2	8,4
62109	57.00N 0.00E	9770	0,96	0,95	0,97	1,06	-0,19	0,89	0,03	0,83	0,21	4,1	5,3	4,3	5,6	3,8	5
62112	58.70N 1.30E	10216	0,94	0,92	0,97	1,03	0,12	0,84	0,32	0,8	0,25	4,5	6,3	5,1	6,8	4,3	5,9
62132	56.50N 2.09E	6719	0,96	0,94	0,97	1	0,04	0,83	0,24	0,81	0,24	4,2	5,5	4,4	5,7	3,9	5,1
62133	57.20N 1.00E	5953	0,96	0,95	0,97	1,09	0,08	0,9	0,27	0,81	0,23	4	5,2	4,6	5,8	4	5,1
62145	53.10N 2.80E	4394	0,95	0,92	0,94	1,04	0	0,91	0,14	0,85	0,18	3	4	3,3	4,3	3,1	4,1
62162	57.40N 0.50E	5989	0,97	0,95	0,97	1,05	0,01	0,86	0,22	0,81	0,24	4,3	5,5	4,6	5,8	4	5,1
62164	57.20N 0.80E	1309	0,96	0,95	0,97	1,08	0,03	0,87	0,22	0,79	0,22	3,6	5	4	5,4	3,4	4,5
62303	51.60N 5.10W	6114	0,96	0,89	0,92	1,05	-0,1	0,61	0,11	0,58	0,17	4,1	5,3	4,3	5,7	2,8	3,7
62305	50.40N 0.00E	11813	0,93	0,82	0,82	1,2	0,19	0,96	0,59	0,75	0,51	2,5	3,6	3,3	4,5	3,3	4,5
62403	53.20N 3.20E	5509	0,95	0,91	0,93	1,09	0,01	0,97	0,14	0,87	0,17	3,1	4,1	3,6	4,8	3,4	4,5
62413	51.90N 3.20E	5521	0,95	0,89	0,91	1,13	-0,13	0,95	0,13	0,82	0,26	2,9	3,8	3,3	4,5	3,1	4,1
63103	61.10N 1.10E	9347	0,97	0,95	0,96	0,97	0,08	0,87	0,36	0,87	0,34	5,8	7,5	5,9	7,5	5,6	7,2
63108	60.80N 1.70E	7434	0,95	0,92	0,94	1,03	0,05	0,91	0,39	0,86	0,4	5,2	6,8	5,6	7,3	5,3	7,1
63111	59.50N 1.50E	10538	0,94	0,92	0,96	1	0,15	0,85	0,38	0,84	0,29	5,1	6,7	5,4	7,2	4,9	6,6
63113	61.00N 1.70E	2239	0,96	0,93	0,95	1,03	0,01	0,91	0,28	0,86	0,31	4,7	6,3	4,9	6,6	4,7	6
63114	61.10N 1.10E	1350	0,97	0,96	0,97	0,94	0,09	0,81	0,28	0,84	0,24	5,8	8,1	5,6	7,8	5,1	6,6
64045	59.00N 11.50W	10982	0,97	0,97	0,98	1	-0,16	0,85	0,2	0,83	0,4	6,6	8,8	6,7	8,9	6	7,8
64046	60.50N 5.00W	2715	0,96	0,97	0,98	0,98	0,03	0,81	0,34	0,8	0,39	6,7	8,5	6,7	8,5	5,8	7,1
LDWR	66.14N 1.80E	7791	0,95	0,95	0,97	1,04	0,17	0,87	0,37	0,81	0,3	5,5	7,4	6,1	8,1	5,3	6,9
LF3F	64.30N 7.80E	6152	0,94	0,94	0,96	0,96	0,19	0,76	0,36	0,76	0,29	6	8	6,2	8,5	5,1	6,9
LF3J	61.20N 2.30E	10168	0,96	0,93	0,96	1	0,12	0,83	0,43	0,83	0,35	5,9	7,6	6,1	8	5,5	7,2
LF3N	65.30N 7.30E	6074	0,92	0,92	0,97	1,07	-0,1	0,84	0,19	0,76	0,33	5,2	7	5,9	7,8	4,8	6,4
LF4B	60.60N 3.70E	3207	0,92	0,85	0,91	1	0,27	0,76	0,63	0,75	0,47	5,4	6,8	5,9	7,6	5	6,4
LF4C	58.40N 1.90E	6924	0,92	0,89	0,97	0,94	0,3	0,75	0,49	0,8	0,24	5	6,5	5,3	6,8	4,6	5,7
LF5U	56.50N 3.20E	9619	0,96	0,94	0,97	1,01	0,02	0,83	0,21	0,82	0,21	4,5	6,2	4,7	6,5	4,1	5,7
TFBLK	65.70N 24.80W	527	0,93	0,91	0,92	0,91	0,01	0,71	0,4	0,74	0,46	4,4	5,1	4	5,2	3,6	4,4
TFDRN	65.80N 21.20W	493	0,95	0,87	0,87	0,9	0,12	0,49	0,15	0,52	0,11	3,5	6,2	3,3	5,4	2	3,5
TFGSK	64.10N 22.90W	463	0,95	0,93	0,92	0,87	0,15	0,78	0,49	0,85	0,44	3,9	5,5	3,6	5,2	3,6	5,2
TFKGR	65.60N 13.60W	454	0,93	0,9	0,86	0,99	-0,01	0,83	0,54	0,75	0,69	3,4	5,1	3,4	5,4	3,3	4,7
TFSRT	63.30N 20.30W	574	0,95	0,93	0,91	0,92	0,12	0,77	0,49	0,78	0,52	4,2	5,6	4	5,2	3,9	5,3

In extreme analysis the accuracy of the data is particularly important at the high end of the empirical density function (EDF). Figure 4 presents the comparisons of the 95- and 99-percentile obtained from the two reanalysis compared to observations. Once again the NORA10 proves better than the ERA40 with its higher correlation and better regression line. Overall, the NORA10 is slightly high, with a mean percentage bias of ~6% (mean absolute bias: ~8%) compared to observations, while the ERA40 is low with about -4% (mean absolute bias: ~10%). One interpretation of the regression analysis is that the NORA10 is slightly high in areas with smaller wave climate, while ERA 40 is low in areas with higher wave climate.

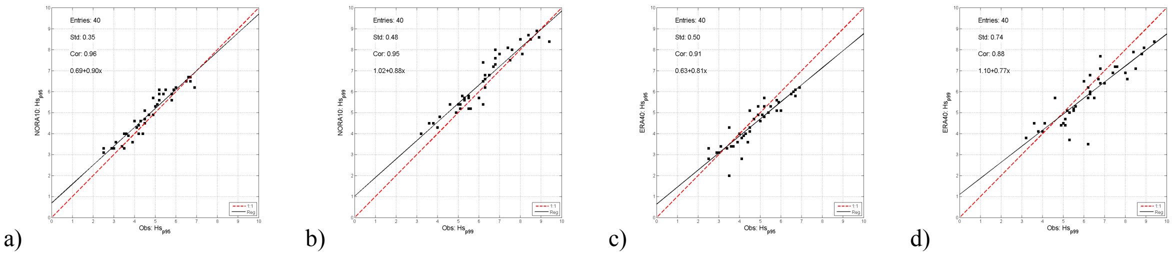

Figure 4: Model performance of the 95 and 99 percentile of significant wave height compared to observations. NORA10: a) 95% and b) 99%. ERA40: c) 95% and d) 99%.

b. Extreme analysis

A reanalysis of the wave field covering a period of 45 years is certainly providing an intriguing data set in respect to extreme analysis. However, any estimated return values based on such a data set needs to be related to the actual wave conditions, i.e. observations. It is somewhat of a paradox though, that we can recreate the temporal and spatial evolution of the wave field without holding a single time series of H_s covering the entire ERA40 period. Still, we are forced to employ the data at hand.

First, we want to establish the data subset, IDM, POT85, POT90 and POT95, which yields the overall best fit between the theoretical CDF, represented by the Gumbel distribution, and the EDF based on both types of data, observations and model. This fit will primarily depend on the location, but will also vary with the type of data. Notice that observations from the five coastal locations near Iceland have been excluded in the succeeding analysis as the total amount of data is too small.

Figure 5 shows an example on how the Gumbel distribution conform to the EDFs based on data selected by the IDM, POT85, POT90 and POT95 at location 62109. These probability plots provide a fair average representation on how the four different data selections influence the behaviour of the CDF and how well it conform to the EDFs at all locations. It is evident that the IDM yields a poor fit at the high end of the distribution, i.e. producing a relative conservative extreme estimate. We found that the IDM offers similar results at about 50% of the 35 locations. Now, by utilizing the POT method we see a clear decrease in the estimated H_s100 and a better fit at the upper tail. However, it is not easy separating the best fit using the different POT data. As noted in Lopatoukhin (2000) the higher the threshold, the smaller the final estimate. Going from POT85 to POT95 there is a difference of -0.4 m at location 62109 using NORA10 data (upper row). On average this bias is -0.75m, which also equals the absolute bias, as the H_s100 based in the POT85 is without exception higher than the same estimates based on POT95. It should be added that the IDM data occasionally conform a very well, but in the same cases the POT approach also seems to provide a reasonable fit between the data and the CDF. Table 2 summarizes the H_s100 estimates based on the different data subsets at each location.

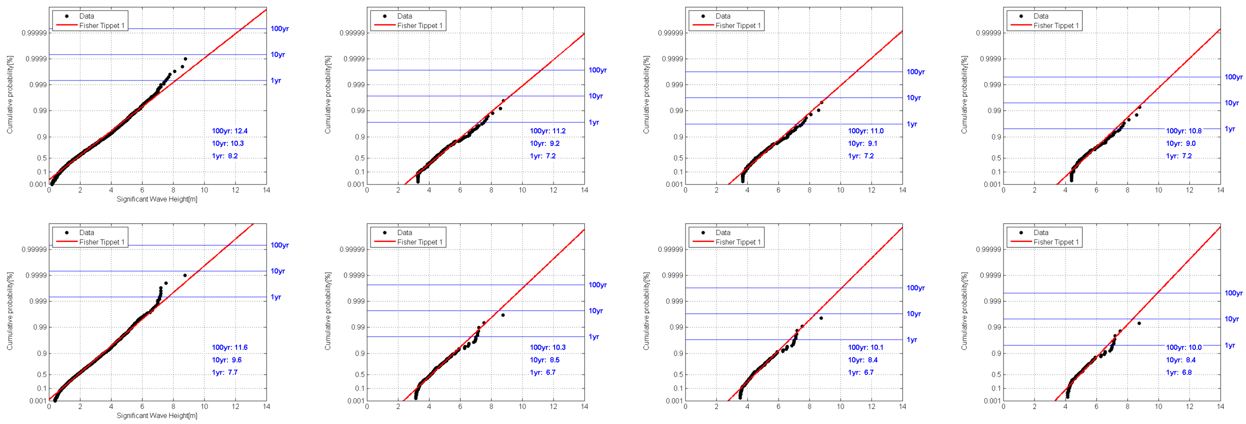

Figure 5: Probability plots for location 62109: Top: NORA10. Bottom: Observations. From left to right: IDM, POT85, POT90 and POT95.

Table 2: *Hs100* estimates based on the Gumbel distribution conformed to IDM-, POT85-, POT90- and POT95-data for the collocated data.

Location	IDM				POT85						POT90						POT95					
		Obs	N10	E40	Obs		N10		E40		Obs		N10		E40		Obs		N10		E40	
	n	X_{100}	X_{100}	X_{100}	n	X_{100}	n	X_{100}	n	X_{100}	n	X_{100}	n	X_{100}	n	X_{100}	n	X_{100}	n	X_{100}	n	X_{100}
3FYT	8156	13,8	16,3	13,5	237	11,6	210	14,7	166	11,7	187	11,1	162	14,3	138	11,3	121	10,6	108	13,5	97	10,8
62023	3672	12,8	12,9	13,7	80	12	72	11	72	11,8	71	12,2	63	10,6	53	11,6	44	11,5	41	10,3	36	10,4
62026	5313	10,4	11	9,5	144	9,9	130	10,9	120	9,2	114	9,7	100	10,7	100	8,9	69	9,2	68	10,2	69	8,7
62090	1937	14,1	16,7	15,3	43	13,6	43	15,7	36	14,2	33	13,3	30	15,4	29	15,5	21	12,2	20	13,7	17	14,3
62091	1925	7,3	9,5	7,9	57	6,4	45	9,6	42	7,3	42	6,1	39	9,3	30	7,1	32	5,9	22	9,4	19	6,8
62103	13526	10,1	11,6	12	339	9,4	290	11,4	247	11,5	274	9,3	207	11,3	193	11,4	165	8,9	138	11	120	10,9
62105	5903	18,3	18,1	16,4	147	16,5	129	16,5	120	14,7	109	16	106	16,1	97	14,5	73	15,6	70	15,6	59	13,9
62106	9389	17,8	18,3	16,1	243	16,4	222	17,5	217	14,9	197	16,2	177	17,2	163	14,9	120	15,8	109	17	103	14,8
62107	8779	13,6	13,5	14,3	191	12,3	160	11,8	157	12,7	143	12	126	11,5	122	12,3	95	11	83	10,6	82	11,8
62108	6410	18,9	17	16,8	147	17,8	135	15,7	134	16,3	117	17,6	106	15,8	114	16,2	78	17	67	14,9	67	15,7
62109	9770	11,6	12,4	10,8	287	10,3	242	11,2	257	9,6	219	10,1	209	11	207	9,4	139	10	134	10,8	128	9,3
62112	10216	13,5	14,8	12,4	255	13	250	13,4	255	11,3	228	12,8	218	13,1	203	11,2	140	12,9	126	13	127	11,2
62132	6719	12,1	12,6	10,8	245	11,7	202	12,2	207	10,1	169	11,7	163	11,9	160	10	115	11,6	103	11,8	101	9,8
62133	5953	11,5	13,1	11,1	164	10,8	142	12,5	141	10,3	129	10,6	118	12,3	117	10	84	10,5	81	12,2	79	10,1
62145	4394	8,9	9,6	8,8	125	8,1	109	8,7	98	8	99	7,9	98	8,4	81	7,8	66	7,7	60	8,1	53	7,4
62162	5989	12,2	13,1	11,1	174	10,9	157	12,2	146	9,9	132	10,7	140	11,9	123	9,7	86	10,6	79	11,9	75	9,8
62164	1309	10,1	11,3	9,4	36	10,4	38	11,2	31	9,5	25	10,1	29	11	23	9,2	15	9,2	16	10,2	16	9
62303	6114	11,8	12,7	8	133	10,8	123	11,3	122	7,6	103	10,3	99	11,2	104	7,4	75	9,8	70	10,7	71	7,1
62305	11813	7,6	9,8	9,3	326	8	275	9,7	199	8,9	244	7,8	204	9,5	154	8,7	161	7,4	133	9,1	101	8,4
62403	5509	9,1	10,4	9,7	155	8,3	132	9,7	136	9,3	118	8,1	103	9,5	91	9,2	83	7,6	67	9	62	9,1
62413	5521	8,3	9,7	8,9	146	7,7	141	9,5	137	8,7	108	7,4	115	9,2	91	8,5	69	7,1	61	8,8	59	8,3
63103	9347	16,6	16,7	15,4	260	14,9	245	15,2	220	13,8	203	14,4	183	14,7	168	13,6	132	13,9	127	14,3	106	13,3
63108	7434	14,8	16	14,9	280	13,8	265	14,3	218	13,2	208	13,5	201	13,9	181	12,9	123	13,2	124	13,6	101	12,8
63111	10538	14,6	15,5	13,8	282	12,8	277	13,7	248	12,2	225	12,6	206	13,5	190	12,1	137	12,2	126	13,3	123	11,9
63113	2239	12,9	13,8	12,7	54	12,6	55	13,2	50	12,2	44	12,1	42	12,8	39	11,8	33	11,8	33	12,2	26	11,7
63114	1350	16,9	16,4	14,4	57	16,5	58	15,8	53	12,4	47	16,3	48	16	47	12,1	36	14,7	37	15,3	36	11,6
64045	10982	18,4	18,9	16,3	284	17,2	276	17,7	248	15	231	16,9	216	17,3	203	14,8	144	16,2	132	16,6	123	14,4
64046	2715	18,8	19	15,9	69	16,1	68	15,9	63	13	56	15,6	56	15,5	54	12,7	44	15,1	34	15,3	38	12,3
LDWR	7791	15,6	17,2	14,6	210	16	192	16,7	182	13,7	171	15,6	151	16,2	148	13,4	105	15,1	104	15,5	97	13
LF3F	6152	17,2	17,6	14	171	15,9	174	17,2	172	14	137	15,3	140	16,7	135	13,7	91	14,6	82	16,1	77	13,4
LF3J	10168	16,7	17,5	15,3	264	14,8	245	15,9	238	13,6	213	14,4	199	15,5	189	13,3	146	14,1	136	15,2	118	13,1
LF3N	6074	14,5	16,5	13,2	163	14	142	15,9	134	12,8	131	13,8	115	15,3	103	12,5	82	13,3	73	14	72	11,7
LF4B	3207	14,7	16	13,4	104	12,1	98	14,9	77	12	87	11,8	73	14,6	66	11,6	50	11	46	13,9	41	11,4
LF4C	6924	14,4	14,8	12,4	229	11,6	210	12,5	212	10,6	174	11,4	161	12,2	170	10,3	107	11,1	104	11,9	100	10,1
LF5U	9619	13,3	13,9	11,9	278	12,7	253	13,5	245	11,2	221	12,6	186	13,5	183	11,3	136	12,5	124	13,5	114	11,4

Based on a strictly visual assessment of the probability plots, we find that the Gumbel distribution conforms best to the POT90 subsets. This applies both to observations and the hindcast data. It is therefore of great interest to see how the *Hs100* estimates based on *in-situ* data relate to the NORA10 and the ERA40, illustrated in Figure 6. Each entry has been colour coded according to the length of the initial data set, i.e. for 6h data one year has a total of 1461 entries, accounting for leap years. In general, *Hs100* estimates are somewhat low for the ERA40, while we find the opposite result for the NORA10, combined with a stronger linear relation to the observations.

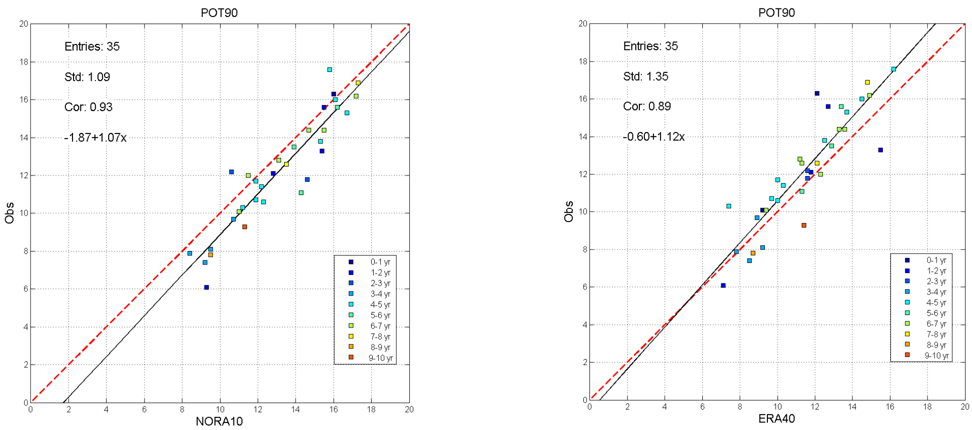

a) b)

Figure 6: Scatter diagrams of estimated *Hs100* based on observations and hindcast data from 35 locations in the Northeast Atlantic. Data are prior to estimation filtered with POT90. The colour coded markers indicate the original amount of data at each location. Left: NORA10. Right: ERA40.

When estimating *Hs100*, it is of special importance that the initial data is equally distributed over an entire year. You do not want a data set overrepresented by e.g. winter values, as this is very likely to produce too high return values. In this analysis, there are three obvious shortcomings in the collocated data set. One, the time series are short. Two, there are gaps in the individual time series. Three, the time series does not cover an integer number of years. So, in other word, any return value estimates solely based on these data sets, must be read with a critical eye. It is however very interesting to see how much the *Hs100* deviates using the same type of data taken from different time periods. Figure 7 shows a scatter diagram of the estimated *Hs100* based on the NORA10 data, where N10-45 is based on the entire ERA40 period while N10 is based on the periods of available observations. First of all, we see a surprisingly strong linear relationship between the two sets of data. Using the POT90 there is a mean absolute percentage bias of 5.5%, while the mean percentage bias is -4.1% for the N10 relative to the N10-45. So, in general the N10 estimates are somewhat low compared to the N10-45. The deviations are still small taking into consideration the very different time spans of some of the time series. As expected, the largest deviations seem to belong to the shorter time series, colour coded in the blue range, while the longer time series, colour coded from green to red, have entries that are closer to the regression line.

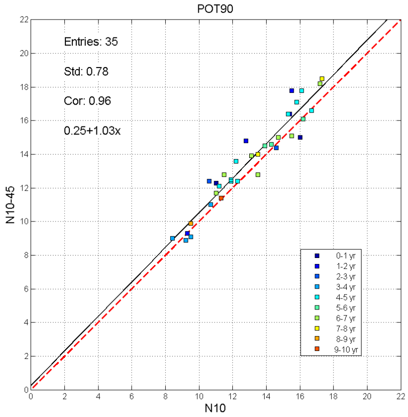

Figure 7: Scatter diagram of *H*s*100* based on NORA10 data using POT95. N10 is based on data from the period of available observations, while N10-45 covers the entire ERA40 period. The colour coded markers indicate the initial amount of data in years of the N10 data.

The validity of the relation found in Figure 6a), i.e.

$$H_{S100}^{Obs} = -1.87 + 1.07 H_{S100}^{NORA10}, \tag{6}$$

is supported by the results illustrated in Figure 7. Even though many of the *in-situ* time series are short in the context of extreme analysis, they prove valid for calibration purposes of *H*s*100*. In the following, we use this linear relation in a more general sense and apply it to the entire model area of the NORA10. Figure 8 shows the *H*s*100* estimates based on 45 years of NORA10 data, filtered by POT90 and adjusted according to eq. 6. The reader should keep in mind that these estimates correspond to 4h means.

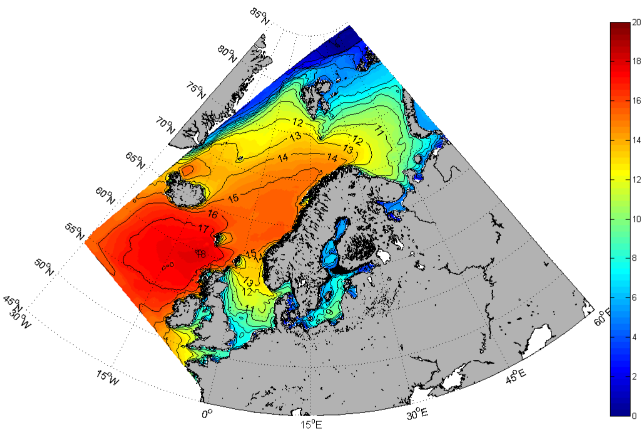

Figure 8: *H*s*100* estimates for the Northeast Atlantic based on the NORA10, filtered by POT90 and adjusted according to eq. 6. The estimates correspond to a 4 hour mean of *H*s.

5. DISCUSSION AND CONCLUSIONS

In this paper we have presented 100-year return value estimates of significant wave height for the Northeast Atlantic. These estimates are obtained using a new regional hindcast, NORA10, developed by the Norwegian Meteorological Institute. The hindcast itself is based on the ERA40 reanalysis, but run with improved temporal and spatial resolution, making it ideal for extreme value analysis on *H*s. Here, NORA10 and ERA40 data have been collocated with *in-situ* measurements at 35 locations. Using a simple regression analysis we extract a linear relation between the return value estimates based on the reanalysis and the observations, motivated by Caires and Sterl (2005). This relation has then been used to calibrate the final result.

All estimates are based on the Gumbel distribution and fitted to data retained with both the initial distribution method (IDM) and the peaks-over-threshold (POT), using different thresholds. Based on a coarse visual assessment we find the IDM unsuitable in about 50% of the cases, where estimates are found too conservative. Generally, the Gumbel distribution seems to conform better to POT-data. Here, the final threshold is set at the 90-percentile of the initial data.

This work utilizes a few easy solutions which need to be addressed:

- It is questionable using a visual assessment to find the most suitable threshold in the POT method, as this is highly subjective. Alternatively, some kind of goodness-of-fit test could be applied, but as stated in Soares and Scotte (2004), most of these techniques are unable to distinguish distributions that are close enough to each other. An alternative solution might be to assess some sort of a relative least-square score for the upper tail. In that way, the threshold may be let to vary over the model domain, depending on the best score.
- All available observations have been used, therefore, the individual time series are unevenly distributed over the year. In addition, some time series contain gaps. Therefore, the H_s100 estimates, based on the periods of collocated data, are often inaccurate for the individual location. A solution would be to cut each time series to only span an integer number of years and fill the gaps with hindcast data. This has not been carried through, as the time series are short to begin with and mixing observations and hindcast data would be questionable as we want to find the relation between the two. Still, using all data might be defended in a first approximation, as we are only interested in the *relation* between H_s100 estimates based on the observations and the NORA10, and not the final H_s100. The fact that all data are collocated in time should prove fare more important.
- In the context of extreme analysis, the relation found between the H_s100 estimates, see eq.6, are based on short time periods. This will diminish the credibility of the final result. However, as illustrated in Figure 7 the differences in the H_s100 estimates based on the NORA10 data taken from the periods of collocated data and the entire ERA40 period are surprisingly small.
- It is highly generalizing conforming one type of CDF to all data. The Gumbel distribution combined with POT-data shows on average a good fit in this work, but might prove inappropriate in other areas and at other water depths. Wimmer *et al.* (2006) proposed a more flexible solution, fitting one of the three candidates included in the family of Generalised Pareto Distribution to POT-data using the maximum likelihood estimation. However, it should be pointed out, that the wave climate at certain locations may belong to more than one distribution, depending on e.g. wave direction, complicating matters even more.

In Caires and Sterl (2005) they found the global maximum south of Iceland to lie between 24.5-27.5m, but probably in the lower part of this interval, see www.knmi.nl/waveatlas/. However, the estimates of this region were found to be excessively high. Focusing on the H_s100 estimates of this work, see Figure 8, we find the same maximum to be approximately 18m. The difference is striking. This may be explained by several factors. One, the final result of the two papers is not directly comparable. In Caires and Sterl (2005) the estimates are representative for sea-states of 2 hours duration, here we use a time window of 4 hours. This will certainly influence the end result. Two, the linear regression between the H_s100 estimates based on observations and NORA10, given by eq. 6, is not well represented by the area of the maximum. The observation density is highest in the northern North Sea, probably making eq. 6 especially adapted for this area. Three, the area of the maximum H_s100 is relatively close to the model boundary where wave conditions are more influenced by the coarser WAM50. Still the NORA10 seems to perform well in the area of the maximum, with the exception of location 62108, where the model clearly underestimates H_s, see Table 1.

The H_s100 estimates of this work seem realistic taking into consideration that the estimates are valid for sea-stats of 4 hours duration. However, in general we consider the estimates low, rather than conservative. It is very important that the reader acknowledge the fact that H_s100 representing sea-states of 1 hour duration would produce higher estimates.

.

Acknowledgment: A big thanks to Jean Bidlot (ECMWF) for providing collocated ERA-40 data and observations.

REFERENCES

Alves, J. H. G. M, and Young, I. R, 2003: On estimating extreme wave heights using Geosat, TOPEX/Poseideon and ERS-1 altimeter data. *Appl. Ocean Res*., **25**, 167-186.

Bjørge, D., Haugen, J. E., Homleid., M., Vigsnes, O. and Ødegaard, V., 2003: Updating the HIRLAM numerical weather prediction system at met.no 2000-2002. Norwegian Meteorological Institute, Research Report No. 145.

Caires, S. and Sterl, A., 2003: Validation of ocean wind and wave data using triple collocation. *J. Geophys. Res.,* **108**, 3098, doi:10.1029/2002JC001491

Caires, S. and A. Sterl, 2005: 100-Year Return Value Estimates for Ocean Wind Speed and Significant Wave Height from the ERA-40 Data. *J. Climate*, **18**, 1032-1048.

Coles, S., 2001: *An introduction to Statistical Modeling of Extreme Values*. Springer-Verlag, 208 pp.

Hagen, Ø., 2009: Estimation of long term extreme waves from storm statistics and initial distribution approach. Proceedings of the 28th International Conference on Offshore Mechanics and Arctic Engineering, OMAE2009-80038.

Komen, G.J., Cavaleri, L., Donelan, M., Hasselmann, K., Hasselmann, S., and Janssen, P. A. E. M. :1994: *Dynamics and Modelling of Ocean Waves*. Cambridge University Press, Cambridge.

Lopatoukhin, L., Rozhkov, V., Ryabinin, V., Swail, V., Boukhanovsky, A., Degtyarev, A., 2000: Estimation of Extreme Wind Wave Heights. World Meteorological Organization. Tech. Rep. 9.

Mathiesen, M., Goda, Y., Hawkes, P., Mansard, E., Martin, M.J., Peltier, E., Thompson, E., and van Vledder, G., 1994: Recommended practice for extreme wave analysis. *Journal of Hydraulic Research* **32** 6, pp. 803–814.

Reistad, M., Breivik, Ø., Haakenstad, H., 2007. A high-resolution hindcast study for the North Sea, the Norwegian Sea and the Barents Sea. Proceedings of the 10th International Workshop on Wave Hindcast and Forcasting and Coastal Hazard Symposium, p. 13.

Saetra, O. and Bidlot, J. R., 2004: On the potential benefit of using probabilistic forecast for waves and marine winds based on the ECMWF ensemble prediction system. *Wea. Forecasting* **19**, pp. 673-689.

Soares, C. G. and Scotto, M. G., 2004: Application of the *r* largest-order statistics for long-term predictions of significant wave height. *Coastal Eng.,* **51,** 387-394.

Uppala, S.M., Kllberg, P., Simmons, A., Andrae, U., da Costa Bechtold, V., Fiorino, M., Gibson, J., Haseler, J., Hernandez, A., Kelly, G., Li, X., Onogi, K., Saarinen, S., Sokka, N., Allan, R., Andersson, E., Arpe, K., Balmaseda, M., Beljaars, A., van de Berg, L., Bidlot, J., an S. Caires, N.B., Chevallier, F., Dethof, A., Dragosavac, M., Fisher, M., Fuentes, M., Hagemann, S., Hlm, E., Hoskins, B., Isaksen, L., Janssen, P., Jenne, R., McNally, A., Mahfouf, J., Morcrette, J., Rayner, N., Saunders, R., Simon, P., Sterl, A., Trenberth, K., Untch, A., Vasiljevic, D., Viterbo, P., and Woollen, J., 2005. The Era-40 re-analysis. *Q. J. R. Meteorol. Soc.* **131**, 2961–3012.

Wimmer, W., Challenor, P., Retzler, C., 2006: Extreme wave heights in the North Atlantic from Altimeter Data. *Renewable Eneregy*, **31**, 241-248.

WMO, 1998: Guide to wave analysis and forecasting. 2nd ed. WMO-No. 702, ISBN 92-63-12702-6